Catalysis Today 175 (2011) 83–92

Contents lists available at ScienceDirect

Catalysis Today

journal homepage: www.elsevier.com/locate/cattod

The effect of regeneration conditions on the selectivity of NO_x reduction in a fully formulated lean NO_x trap catalyst

Jin Wang[a], Yaying Ji[a], Vencon Easterling[a], Mark Crocker[a,*], Mark Dearth[b], Robert W. McCabe[b]

[a] Center for Applied Energy Research, University of Kentucky, Lexington, KY 40511, USA
[b] Chemical Engineering Department, Ford Motor Co., Dearborn, MI 48124, USA

ARTICLE INFO

Article history:
Received 22 October 2010
Received in revised form 25 January 2011
Accepted 26 February 2011
Available online 1 April 2011

Keywords:
Lean NO_x trap
NO_x storage/reduction catalyst
Ammonia
Selectivity
Reductant
SpaciMS

ABSTRACT

The effect of regeneration conditions on NH_3 formation in a fully formulated Pt–Rh/BaO/Al_2O_3 lean NO_x trap catalyst was investigated. Experiments were performed on a bench flow reactor under simulated diesel exhaust conditions, employing NO_x storage/reduction cycles. Using CO/H_2 as the reductant, the selectivity of NO_x reduction to NH_3 increased with increasing regeneration time, reductant concentration and space velocity, and decreased with increasing amount of stored NO_x and increasing temperature. At a given temperature the effect of these parameters on NH_3 selectivity can be interpreted in terms of the local H_2:NO_x ratio at the precious metal sites and the extent to which NH_3 is consumed in the reductant front as it propagates through the catalyst. However, selectivity to NH_3 increased with increasing temperature (>300 °C) during rich purging using C_3H_6 as the reducing agent. It was shown that NH_3 selectivity was governed by the steam reforming activity of the catalyst, selectivity to NH_3 increasing with increasing H_2 generation. Experiments using a second catalyst to which ceria had been added as an OSC material confirmed these trends, although the presence of the ceria resulted in lower selectivity to NH_3 when using H_2 and/or CO as the reductant. After aging, the catalysts displayed increased selectivity to NH_3; this is attributed in part to lengthening of the NO_x storage-reduction zone, as demonstrated by SpaciMS data, and decreased OSC, resulting in decreased NH_3 consumption by NO_x and O_2 downstream of the reductant front.

1. Introduction

Lean-burn engines provide more efficient fuel combustion and lower CO_2 emissions compared with traditional stoichiometric engines. However, the effective removal of NO_x from lean exhaust represents a challenge to the automotive industry. In this context, lean NO_x traps (LNTs), also known as NO_x storage-reduction (NSR) catalysts, represent a promising technology, particularly for light duty diesel and gasoline lean-burn applications. Moreover, recent studies have shown that the performance of LNTs can be significantly improved by adding a selective catalytic reduction (SCR) catalyst in series downstream [1–18]. SCR catalysts promote the selective reduction of NO_x with ammonia (NH_3) in the presence of excess oxygen. In the combined LNT–SCR system, NH_3 is generated in the upstream LNT during rich purges and subsequently stored on the SCR catalyst where it reacts with NO_x that breaks through the LNT during lean operation. This contrasts with active SCR systems in which NH_3 is typically generated from urea carried on-board the vehicle. Compared to an LNT-only system, the LNT–SCR system has several advantages. First, the SCR catalyst eliminates NH_3 slip from the LNT by storing it and subsequently catalyzing its reaction with unreacted NO_x from the LNT. Second, the presence of the SCR catalyst relaxes the NO_x conversion requirements of the LNT. Consequently, the LNT catalyst volume in the LNT–SCR system can be lower than for an LNT-only system, reducing the precious metal costs for the system [12].

Neither the optimal engine control strategy nor the optimal catalyst formulations for generating and reacting NH_3 in an LNT + in situ SCR application is obvious, however. NH_3 generation is the result of deep, rich purges of the LNT, which comes at the price of fuel economy. Thus there is a need to identify LNT and SCR formulations and reductant injection strategies that optimize NH_3 generation, storage, and reaction with NO_x to enhance overall NO_x conversion, while minimizing fuel consumption. Towards the goal of optimizing LNT–SCR system performance, this study seeks to elucidate the influence of a range of process parameters on the selectivity of NO_x reduction to NH_3 in a fully formulated LNT catalyst. In this context, we note that several previous studies have addressed the issue of product selectivity during LNT catalyst regeneration. Pihl et al. [19] performed pseudo-steady state continuous flow experiments using a commercial LNT and found that selectivity to NH_3 increased with higher reductant concentrations

* Corresponding author. Tel.: +1 859 257 0295; fax: +1 859 257 0302.
E-mail address: crocker@caer.uky.edu (M. Crocker).

0920-5861/$ – see front matter © 2011 Elsevier B.V. All rights reserved.
doi:10.1016/j.cattod.2011.02.048

Table 1
Composition of catalysts used in this study[a].

Component	Catalyst code/loading	
	30-0	30-50
Pt, g/L	3.53	3.53
Rh, g/L	0.71	0.71
BaO, g/L	30	30
CeO_2 [b], g/L	0	50
Al_2O_3 [c], g/L	Balance	Balance

[a] Nominal loadings. Total washcoat loading = 260 g/L.
[b] Stabilized with 5 wt% La_2O_3.
[c] Stabilized with 3 wt% La_2O_3.

Table 2
Base conditions used for NO_x storage-reduction cycling experiments[a].

Parameter	Lean	Rich
Duration, s	60	5
Temperature (°C)	200–400	200–400
NO, ppm	300	0
O_2, %	10	0
H_2, %	0	1.3
CO, %	0	4
H_2O, %	5	5
CO_2, %	5	5
N_2, %	Balance	Balance

[a] GHSV = 30,000 h^{-1} for all conditions.

(i.e., increasing H_2:NO and CO:NO ratio) and lower temperatures. Related experiments showed that NH_3 was readily oxidized by both NO and O_2 over the catalyst. Similarly, using model catalysts, Xu et al. [20] and Clayton et al. [21] showed that the selectivity of NO reduction by H_2 (to N_2O, N_2 and NH_3) is largely dictated by the H_2:NO ratio and temperature under steady-state conditions. These findings are consistent with a study of NO reduction by H_2 on Pt–Rh single crystal surfaces [22], which concluded that the selectivity of the reaction is determined by the relative amounts of H_2, NO and N adatoms on the surface. Using an engine test-bench, Hackenberg and Ranalli [23] studied the dependence of NO_x reduction selectivity on NO_x loading, regeneration time, rich phase lambda and hydrocarbon injection. NH_3 formation was found to be dependent on regeneration time and the air-fuel ratio but was not influenced by the amount of stored NO_x. The use of post-injection of hydrocarbons into the exhaust to assist engine-based regeneration resulted in a significant increase in NH_3 formation. In contrast, Nova et al. [24] found that NH_3 formation is dependent on the amount of stored of NO_x, as did Abdul-Milh and Westberg [25], in addition to temperature and H_2 concentration. Additionally, several other research groups [26,27] have reported that LNT selectivity to NH_3 increases with increasing rich purge duration and reductant concentration.

In the present paper we report the results of a study concerning the effect of reductant concentration and type, purge length, amount of stored NO_x, and space velocity on the selectivity of NO_x reduction to NH_3. Given that we have previously observed that catalyst oxygen storage capacity (OSC) can influence the selectivity of NO_x reduction [28–30], the effect of catalyst OSC was also considered in this study by employing two catalysts, one of which contained an OSC material (ceria) while the other did not. In order to rationalize the observed dependencies, we also present the results of related continuous flow and SpaciMS (spatially resolved capillary inlet mass spectrometry) measurements.

2. Experimental

2.1. Catalyst preparation and characterization

Two fully formulated Ba-based LNT catalysts were used in this study, the compositions of which are shown in Table 1. Details of the catalyst preparation have been described elsewhere [29]. In both cases, the washcoat was applied to a 4″ × 6″ cordierite monolith substrate, possessing a cell density of 400 cpsi and a wall thickness of 6.5 mil. As shown in the table, the catalysts have the same nominal loadings of Pt, Rh and BaO, differing only in the loading of La-stabilized CeO_2. The BaO component (21.5 wt%) was supported on alumina, while bare alumina was also used as balance to bring the total washcoat loading up to 260 g/L.

Surface area and pore volume measurements on the fresh and aged catalysts were performed according to the BET method by nitrogen adsorption at −196 °C using a Micromeritics Tri-Star system. Prior to the measurements catalyst samples (washcoat and monolith) were ground to a fine powder and outgassed overnight at 160 °C under vacuum. The dispersion of precious metal (Pt + Rh) was determined with a Micromeritics AutoChem II Analyzer by means of pulsed H_2 chemisorption at dry ice temperature (−78 °C). OSC values of the catalysts were determined under lean-rich cycling conditions as described previously [29].

2.2. Catalyst aging

Catalyst aging was performed on a synthetic gas bench using cores (2.1 cm diameter × 7.4 cm long) drilled out from the LNT monoliths. The protocol used for the rapid aging has been detailed in earlier publications [12,30]. This method is designed to simulate the road aging of a LNT catalyst used in conjunction with a diesel particulate filter (DPF). Each aging cycle is composed of three modes: sulfation, desulfation, and simulated DPF regeneration. A maximum mid-bed catalyst temperature of 770 ± 10 °C was observed during desulfation due to the exotherm resulting from the fast lean-rich cycling. Depending on actual fuel sulfur levels, one aging cycle is estimated to be equivalent to 1000–1500 miles of road aging. 50 cycles were used for the aging runs, requiring a total aging time of ca. 100 h per sample.

2.3. Lean-rich cycling experiments

Catalyst tests using monolithic samples were performed on a synthetic gas bench reactor. Catalyst cores were wrapped in Zetex insulation tape and inserted into a vertical reactor tube (2.2 cm inner diameter). The reactor tube was heated by an electric furnace, and simulated exhaust gas mixtures were introduced from pressurized gas bottles. Water was introduced by a peristaltic cartridge pump (Cole-Parmer) to a heated zone, vaporized and added to the simulated exhaust mixture. A rapid switching 4-way valve system was used to alternate between the lean and rich gas mixtures so that the lean/rich/lean transitions in these experiments were almost instantaneous (within 0.2 s). Three K-type thermocouples were placed just before the LNT, at the LNT mid-point and just after the LNT to monitor the temperature profiles. A multigas analyzer (MKS Model 2030) was used to monitor NO, NO_2, N_2O, NH_3, CO, CO_2, H_2O at the reactor outlet. During lean-rich cycling, the observed catalyst breakthrough profiles stabilized to a fixed limit cycle in about 2 h, at which point it was possible to characterize the performance in terms of the 'stationary' concentration cycles. The base conditions for the cycling experiments are summarized in Table 2; in order investigate the effect of the different process parameters on the selectivity of NO_x reduction to NH_3, the parameters in question were sequentially varied, while the other parameters were fixed at these base values. The selectivity to N_2 during rich purges was determined by difference (i.e., $S_{N_2} = 100\% - S_{N_2O} - S_{NH_3}$). In the case of measurements performed on fresh catalysts, the samples were in all cases first de-greened

by exposing them to lean-rich cycling conditions at 500 °C for 5 h.

2.4. Temperature ramp experiments

Temperature ramp experiments were performed using 2.1 cm × 2.54 cm ($d \times l$) catalyst cores operating at a higher Gas Hourly Space Velocity (GHSV; 120,000 h^{-1}) than the cycling experiments (30,000 h^{-1}) in order to ensure a fast approach to steady-state. The catalyst was allowed to equilibrate under the gas flow at 125 °C, after which the temperature was ramped to 500 °C at a rate of 5 °C min^{-1}.

2.5. Temperature programmed steam reforming and NO reduction experiments

Steam reforming tests were performed in a U-shape quartz tube (inlet 10 mm I.D. and outlet 3 mm I.D.) connected to a mass spectrometer (Pfeiffer Thermostar GSD301) for the continuous on-line analysis of the outlet gases. 100 mg of crushed monolithic catalyst in the form of small particles (100–120 μm) and a total gas flow of 120 sccm were used in each run. Before each experiment, catalysts were pretreated at 500 °C for 15 min under a flowing gas mixture containing 10% H_2, 5% CO_2, 3% H_2O and Ar (balance). After cooling to 150 °C, the gas flow was switched to one containing 5000 ppm C_3H_6, 5% CO_2, 3% H_2O and He (balance) and the temperature was ramped to 500 °C at a rate of 5 °C min^{-1}. The temperature of the catalyst was measured and controlled by a K-type thermocouple directly immersed in the catalyst bed. The following mass-to-charge ratios were used to monitor the concentration of products and reactants: 2 (H_2), 15 (NH_3), 28 (N_2 or CO), 30 (NO), 32 (O_2), and 41 (C_3H_6). The mass spectrometer data were quantitatively analyzed using the fragmentation patterns and the response factors determined experimentally from calibration gases. Relevant interferences in the mass-to charge signals were taken into account in determining the product composition. Temperature programmed NO reduction experiments with C_3H_6 were performed similarly, using a feed gas consisting of 300 ppm NO, 5000 ppm C_3H_6, 5% CO_2, 3% H_2O and He (balance).

2.6. SpaciMS measurements

Catalyst samples for SpaciMS measurements were divided into two groups. In the first group, the samples were de-greened by exposure to flowing gas consisting of 500 ppm NO, 5% CO_2, 5% H_2O, and the balance N_2 at 800 °C for 2 h. The second group was aged by exposure to lean conditions for a period of 24 h at 800 °C, the feed gas consisting of 8% O_2, 500 ppm NO, 5% CO_2, 5% H_2O, and the balance N_2. The catalyst monolith cores measured 1.75 cm × 2.54 cm ($d \times l$), resulting in a GHSV of 30,000 h^{-1}. The samples were subsequently exposed to 60 s lean/5 s rich cycles in a quartz tube reactor at three temperatures (200, 250, and 300 °C). The lean phase gas contained 500 ppm NO, 8% O_2, 5% CO_2, 5% H_2O, and balance N_2, while the rich phase gas contained 4.2% H_2, 1% O_2, 5% CO_2, 5% H_2O, and balance N_2. Prior to the measurements, each sample was exposed to the cycling conditions until the component concentrations in the reactor effluent were constant from one cycle to the next. During this period, a coated fused silica polyamide capillary (SGE Scientific) with a 250 μm outer diameter was positioned near the centerline of the monolith for the purpose of gas sampling, at a location 10 mm from its rear face. Gas was sampled at a rate of 14 cm^3 min^{-1}, its composition being analyzed using a V & F Airsense 2000 chemical ionization mass spectrometer. The measurement time was ~10 ms. The low energy ion source, Hg, was used to identify reaction products. Once "stationary" cycles had been attained, data were collected at different positions measured from the front face of the catalyst. The first of these positions corresponded to the rear face (25.4 mm from the catalyst inlet), with successive sampling at 19.4 mm, 13.4 mm, 7.4 mm, 4.4 mm, and 0.0 mm from the inlet. For each measurement at a given temperature, the system was allowed to stabilize for two 60 s/5 s cycles before data were taken over five successive cycles. These cycles were then averaged to produce the spatio-temporal plots of species concentration versus time for each axial location.

3. Results and discussion

3.1. Catalyst characterization

Extensive characterization data for the two catalysts used in this study have been reported previously [29,31]. For this reason, in Table 3 we report only those data most relevant to this study. As shown, in the fresh state the estimated washcoat BET surface areas for the two catalysts are similar. The surface areas of both catalysts are decreased after aging, that for catalyst 30-50 showing the largest decline. This is consistent with sintering of the ceria component in 30-50 [31], which is also reflected in a significant decrease in OSC, although the OSC of 30-50 remains superior to that of 30-0 after aging. Also noteworthy is the substantial decline in precious metal dispersion that occurs upon aging, based on both H_2 chemisorption and previously reported TEM data [31].

3.2. Effect of rich phase time

Fig. 1 shows the effect of rich phase duration on NO_x conversion and selectivity to NH_3 at different temperatures. From Fig. 1(a) it is apparent that NO_x conversion increases with increasing purge length, albeit that for catalyst 30-50, which is exceptionally active, NO_x conversion reaches close to 100% at 300 and 400 °C at purge times of only 5 s and 7 s, respectively. Fig. 1(b) shows that for both catalysts selectivity to NH_3 increases with increasing rich time and decreases with increasing temperature. Comparing the two catalysts, it is evident that NO_x conversion over 30-50 is always higher than that of 30-0 at the same reaction conditions, whereas the selectivity to NH_3 exhibited by 30-0 is consistently higher than that of 30-50. As we have previously detailed [28–30], the presence of ceria is beneficial for increased NO_x storage capacity, increased water–gas shift activity (favoring in situ generation of H_2), and NO_x reduction activity, all of which contribute to the superior cycle-averaged NO_x conversion displayed by 30-50. The presence of ceria is also expected to affect NH_3 selectivity due to its OSC properties. Specifically, as discussed in the literature [29,32,33], the following effects can be proposed: (i) consumption of the reductant by stored oxygen results in decreased H_2:NO_x ratios during regeneration, which should favor the formation of N_2 over NH_3 (as discussed in Section 3.4) and (ii) oxygen stored in the rear of the catalyst can consume NH_3 formed upstream via oxidation (with N_2, NO and N_2O as the possible products).

3.3. Effect of CO/H_2 concentration

Fig. 2 shows the dependence of NO_x conversion and NH_3 selectivity on different CO/H_2 concentrations for 30-0 as a function of temperature. Catalyst 30-50 exhibited similar trends and so the results are not shown here. From Fig. 2(a) it is apparent that NO_x conversion increases with increasing CO/H_2 concentration, the effect being particularly significant at 200 °C. Evidently, the catalysts are unable to utilize the reductants efficiently at this temperature, this being a consequence of the relatively slow kinetics of NO_x release and reduction at such relatively low temperatures [34]. From Fig. 2(b), NH_3 selectivity is seen to increase with increasing CO/H_2 concentration at each temperature. This result is consistent

Table 3
Physical properties and oxygen storage capacity of fresh and aged catalysts[a].

Catalyst	Estimated washcoat BET SA (m^2/g)[b]		Total BET surface area (m^2/g)		PM dispersion (%)		Oxygen storage capacity (mmol O/L)[c]	
	Fresh	Aged	Fresh	Aged	Aged	Fresh	Fresh	Aged
30-0	121	107	43.5	37.8	34.0	8.5	21.5	19.4
30-50	126	88	47.5	32.7	51.2	9.2	38.1	26.0

[a] Aging protocol as detailed in Section 2.2.
[b] Estimate calculated from washcoat loading and surface area of 1 m^2/g for cordierite substrate.
[c] Measured at 350 °C.

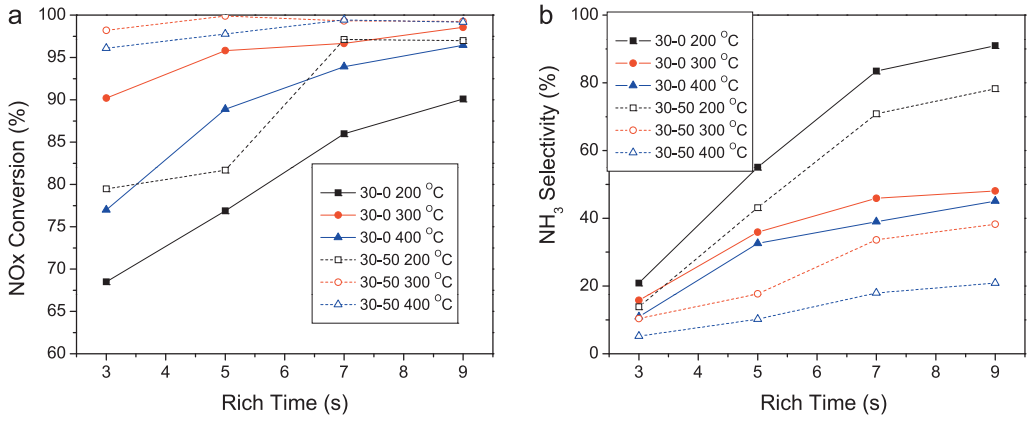

Fig. 1. Dependence of (a) cycle-average NO_x conversion and (b) NH_3 selectivity on regeneration time at different temperatures. Rich phase duration = 3, 5, 7, 9 s; other conditions as for Table 2.

with previous literature reports [20,21,23–26] indicating that the reductant:NO_x ratio is a key factor in determining the selectivity of NO_x reduction during LNT regeneration.

3.4. Steady-state study of NO reduction by H_2

The transient nature of cycling experiments, coupled with the integral nature of monolithic catalysts, make it difficult to directly relate outlet gas composition to the chemistry taking place inside the catalyst. For this reason, the steady-state reaction of NO_x with H_2 was studied in order to examine the sensitivity of the NO_x reduction selectivity to the H_2:NO_x ratio. Fig. 3 shows the results of experiments performed with 30-0 using H_2:NO ratios of 1:1 and 2.5:1. Again, the trends shown by 30-50 are similar and so the results are not shown here. As shown, the NO + H_2 reaction lights off at very low temperatures, NO conversions in excess of 80% being obtained at 50 °C. Fig. 3 also shows that temperature has a strong effect on product composition. NO is reduced to a mixture of all three product species (NH_3, N_2, and N_2O) at low temperatures (<200 °C), whereas the reactions become highly selective towards either NH_3 or N_2 higher temperature (200–500 °C). Specifically, when the mixture is stoichiometric for N_2 generation (H_2:NO = 1:1), the reduction reaction is highly selective towards N_2, whereas when the feed gas ratio is stoichiometric for NH_3 (H_2:NO = 2.5:1), NH_3 is the primary product. Similar results have been reported by Pihl et al. for a commercial LNT [19], and Xu et al. [20] for model catalysts of the Pt/Al_2O_3 and $Pt/BaO/Al_2O_3$ type. Above 375 °C the selectivity to NH_3 drops significantly, an occurrence which can be attributed to the catalyzed decomposition of NH_3 to N_2 and H_2; this was confirmed in separate experiments (data not shown). Overall, these steady-state results are consistent with the lean-rich cycling results presented above and highlight the important role that the reductant:NO_x ratio plays in determining the selectivity of NO_x reduction in LNT catalysts.

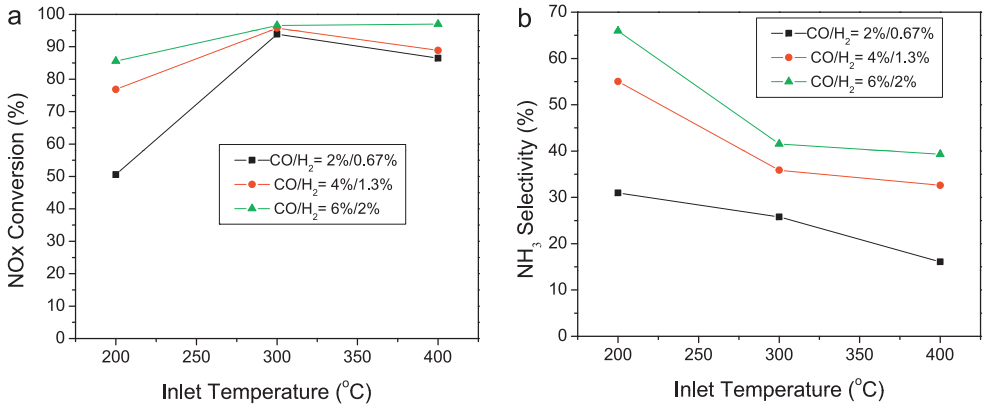

Fig. 2. Dependence of (a) cycle-average NO_x conversion and (b) NH_3 selectivity on reductant (CO + H_2) concentration for catalyst 30-0. Other conditions as for Table 2.

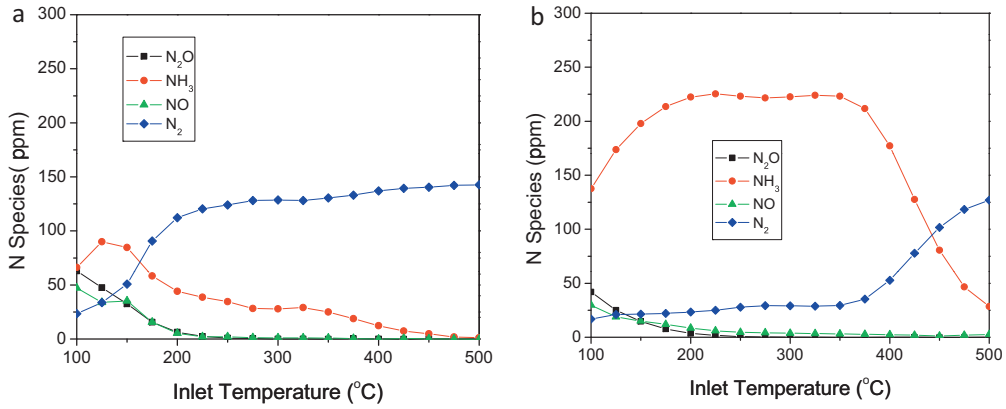

Fig. 3. Steady state reaction of NO + H_2 over catalyst 30-0: (a) H_2:NO = 1:1, (b) H_2:NO = 2.5:1. Conditions: 300 ppm NO, 300 or 750 ppm H_2, 5% CO_2, 5% H_2O, N_2 balance, 120,000 h^{-1} GHSV, and 5 °C min^{-1} ramp rate.

3.5. Effect of NO_x loading

The dependence of selectivity to NH_3 on the amount of NO_x stored is shown for catalyst 30-0 in Fig. 4. In these experiments the amount of NO_x stored was varied by altering the lean phase feed NO_x concentration (at constant lean phase duration). Additional experiments were performed in which the amount of NO_x stored was varied by altering the lean phase duration at constant NO_x concentration in the feed. The data for these latter experiments show identical trends to the first and so are not included in Fig. 4. In both cases the selectivity of NO_x reduction to NH_3 decreases with increasing amount of NO_x stored. While this finding contrasts with the work of Hackenberg and Ranalli [23], it is in agreement with earlier reports by Nova et al. [24] and Abdul-Milh and Westberg [25], who found a clear correlation between NO_x loading and NH_3 selectivity.

3.6. Effect of space velocity

Fig. 5 shows the effect of varying the GHSV on NO_x conversion and NH_3 selectivity for catalyst 30-0. As expected, the NO_x conversion decreases with increasing GHSV (decreasing residence time) at each temperature. Simultaneously, selectivity to NH_3 increases with increasing GHSV. Several possible explanations for this behavior can be advanced, which are considered in Section 3.8.

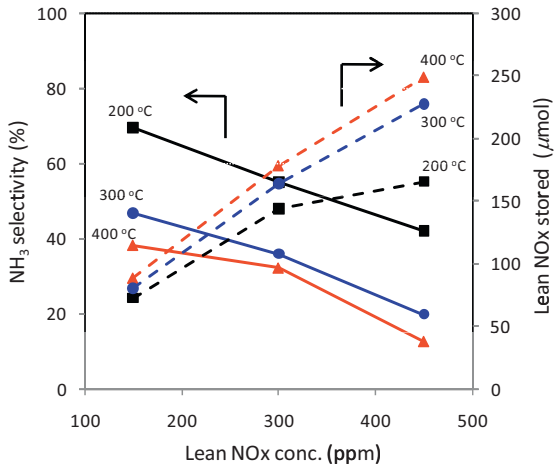

Fig. 4. Dependence of NH_3 selectivity on amount of NO_x stored for catalyst 30-0. Conditions as for Table 2.

3.7. Effect of reductant type

The effect of reductant type on NO_x conversion and NH_3 selectivity was examined for catalysts 30-0 and 30-50 in lean-rich cycling experiments utilizing H_2, CO and C_3H_6 (propene) as the reductant (Fig. 6). From Fig. 6(a) and (b) it is evident that at 200 °C H_2 (1.5%) is a significantly better reductant than CO (1.5%) or C_3H_6 (0.5%). This result is consistent with reports from other researchers [35–40]. However, for catalyst 30-50, at 300 and 400 °C slightly higher NO_x conversion is obtained with C_3H_6 as reductant compared to H_2. Epling and co-workers [40] found that at temperatures of 300 °C and higher, C_3H_6 is as efficient as H_2 and CO in LNT regeneration. The slightly improved activity of 30-50 with 0.5% C_3H_6 is likely related to its very high intrinsic activity, combined with the fact that one molecule of C_3H_6 represents nine reducing equivalents, assuming that it is fully oxidized to CO_2 and H_2O during NO_x reduction. Consequently, the supply of reducing equivalents was greater when using 0.5% C_3H_6 as reductant as compared to 1.5% H_2. The behavior of 30-50 contrasts with that of 30-0, however, which evidently is unable to use C_3H_6 as efficiently as 30-50; consequently, NO_x conversion over 30-0 at 300 and 400 °C is slightly higher with H_2 than C_3H_6. Subtle differences are also observed between 30-0 and 30-50 with respect to the selectivity of NO_x reduction. The most striking feature of the NH_3 selectivity plots (Fig. 6(c) and (d)) is that whereas the selectivity to NH_3 decreases with increasing temperature when H_2 or CO are used as the reductant, the opposite trend is observed with C_3H_6. For both catalysts the selectivity to NH_3 is less than 5% at 200 and 300 °C but becomes significant at 400 °C. However, NH_3 selectivity is higher for 30-50 than 30-0 at both 300 and 400 °C, a trend which contrasts with the findings for LNT regeneration using CO/H_2 mixtures (Fig. 1) and H_2 (Fig. 6(c) and (d)), for which 30-50, possessing higher OSC than 30-0, consistently displays lower NH_3 selectivity.

Suspecting that differences in the steam reforming activity of 30-0 and 30-50 may account for the trends in catalyst behavior observed with C_3H_6, their activity in the stream reforming of C_3H_6 was examined. According to Fig. 7(a), the light-off temperature of 30-50 is at least 50 °C lower than that of 30-0, while 30-50 is also considerably more active than 30-0 for H_2 generation at higher temperatures (>350 °C; see Table 4). These results clearly show that the presence of ceria in catalyst 30-50 promotes the steam reforming reaction of C_3H_6, thereby generating H_2 in situ and facilitating NO_x reduction to NH_3. As shown in Fig. 7(b) for 30-0, when NO is added to the feed gas, significant NO reduction activity is observed in the temperature range 200–250 °C, NO conversion reaching ~80% at 250 °C. Below the on-set of steam reforming (>250 °C), C_3H_6 must participate in NO_x reduction via

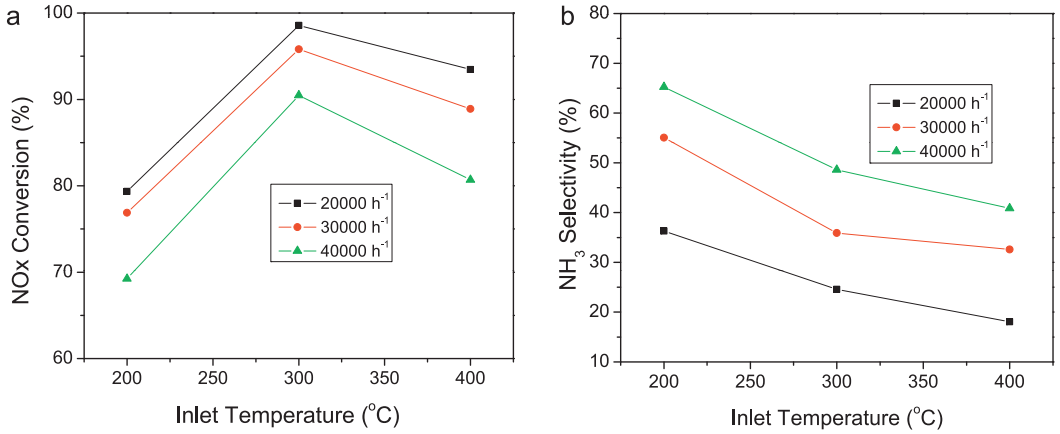

Fig. 5. Dependence of (a) cycle-average NO_x conversion and (b) NH_3 selectivity on GHSV for catalyst 30-0. Other conditions as for Table 2.

other pathways, such as the redox mechanism proposed by Burch et al. [41] (involving NO_x decomposition to N_2 and/or N_2O on precious metal particles, with associated oxygen removal by reaction with C_3H_6), or via the reaction of C_3H_6 with NO_x to form organo-nitrogen species which decompose to afford ultimately N_2 or N_2O [41,42]. Indeed, the relatively low concentrations of H_2 generated over both 30-0 and 30-50 at temperatures below 450 °C indicate that the steam reforming pathway represents a minor route for NO_x reduction by C_3H_6 at typical LNT working temperatures, although it significantly impacts the selectivity of NO_x reduction to NH_3 at 400 °C.

3.8. Qualitative description of LNT regeneration

Any attempt to interpret the data presented in Sections 3.2–3.7 must take into account the integral nature of the catalyst monoliths used in this work. According to the model proposed by Ribeiro and co-workers [43,44], during LNT regeneration a H_2-rich reaction

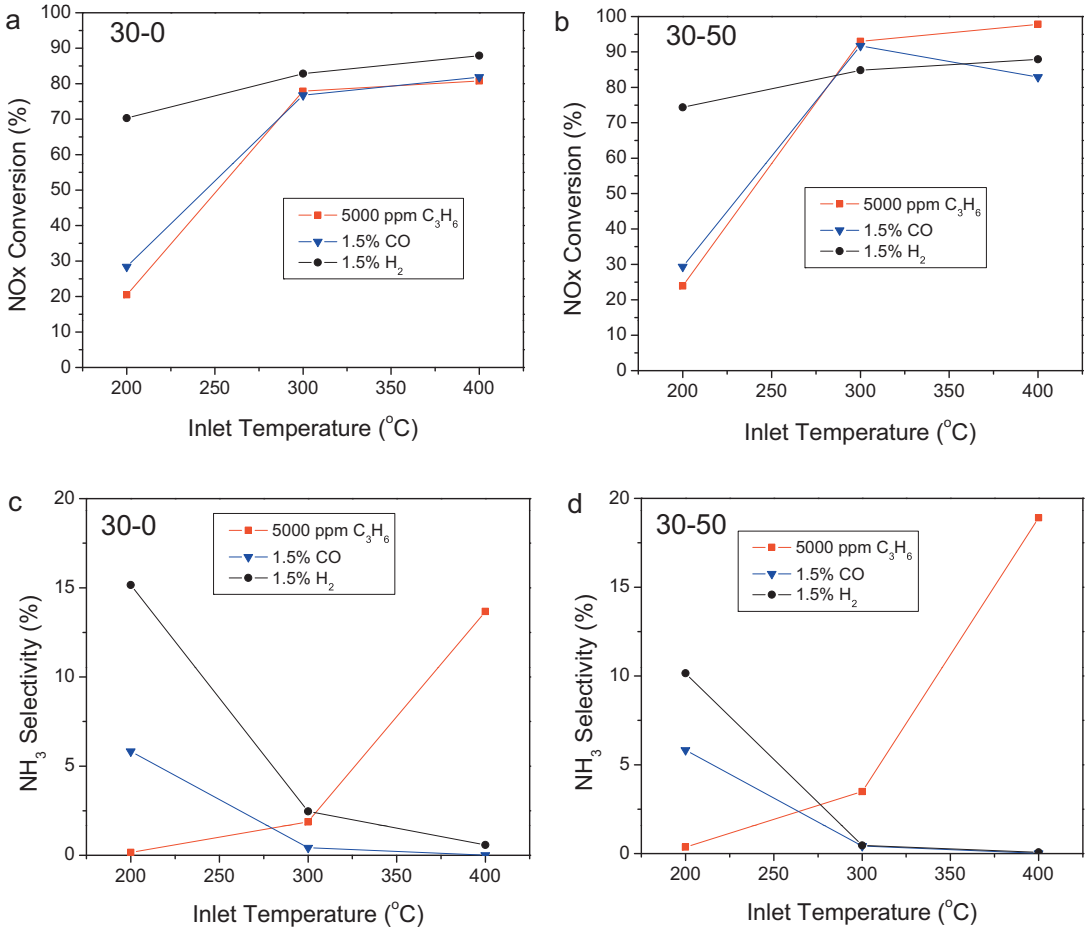

Fig. 6. Dependence of cycle-average NO_x conversion (a and b) and NH_3 selectivity (c and d) on reductant type for catalysts 30-0 and 30-50. Reductant concentrations: 1.5% CO, 1.5% H_2, 5000 ppm C_3H_6; other conditions as for Table 2.

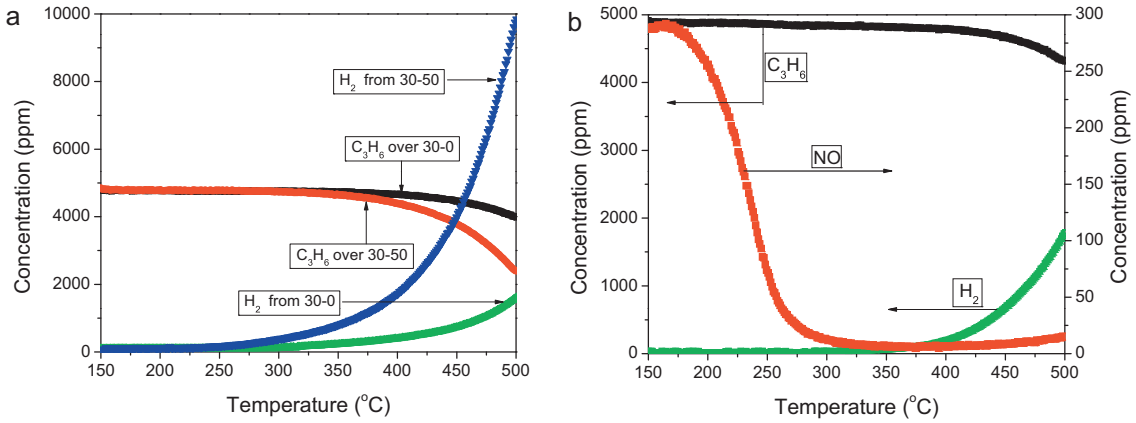

Fig. 7. (a) Comparison of steam reforming activity of catalysts 30-0 and 30-50. Reaction conditions: 5000 ppm C_3H_6, 5% CO_2, 3% H_2O, and He balance. (b) Temperature programmed reduction of NO with C_3H_6 over catalyst 30-0. Conditions as for (a) but with 300 ppm NO added.

Table 4
Steam reforming of C_3H_6 over catalysts 30-0 and 30-50[a].

T (°C)	C_3H_6 conv. (%)		H_2 yield (ppm)	
	30-0	30-50	30-0	30-50
300	1	1	112	397
400	3	8	372	1730
500	17	50	1609	9845

[a] Conditions as for Fig. 7(a).

front propagates along the length of the catalyst in which N_2 and NH_3 are formed from the reduction of the stored NO_x. The formed NH_3 may then react further with nitrates stored downstream of the front, resulting in the formation of N_2. This explains the temporal sequence of product formation, N_2 breakthrough occurring before NH_3; breakthrough of the latter corresponds to the point at which the stored NO_x is sufficiently depleted for the NH_3 consumption to be incomplete. A similar two-step model has been also been proposed by Lietti et al. [17,45]. Direct evidence supporting the existence of parallel direct-H_2 and intermediate-NH_3 regeneration pathways has been provided by SpaciMS measurements [46] and by effluent measurements performed on different length catalysts, from which the evolution of intracatalyst species was reconstructed [47]. In both cases the data are consistent with NH_3 being produced and consumed along the catalyst, thereby functioning as an intermediate reductant. In addition to the NH_3–NO reaction, NH_3 can also be consumed by reaction with stored oxygen as alluded to in Section 3.2, or can undergo decomposition at high temperatures (Section 3.4). Fig. 8 summarizes the complete network of possible reactions involving NH_3.

Considering the effect of the rich phase time on NH_3 selectivity, it is clear that the chemistry occurring in the reductant front will not be affected by the duration of the purge. However, longer purge

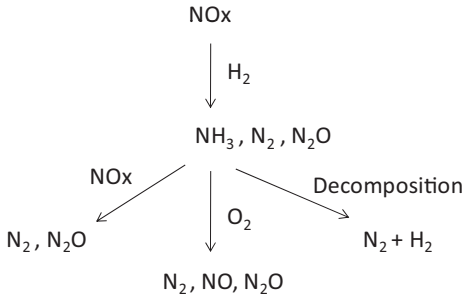

Fig. 8. Schematic showing reaction pathways for NH_3 generation and consumption.

times enable the regeneration of those NO_x storage sites located relatively far away from the Pt and Rh sites, i.e., sites for which diffusion of NO_x within the Ba phase is rate limiting (as opposed to the feed rate of reductants to the Pt or Rh sites). Regeneration of these sites will occur behind the leading edge of the reductant front, giving rise to high local H_2:NO_x ratios which favor NH_3 formation. Furthermore, NH_3 formed behind the front is less likely to be subsequently consumed than NH_3 formed in the front, given the lower concentrations of adsorbed NO_x remaining behind the front.

The effect of reductant concentration on NH_3 selectivity can be expected to manifest itself in two ways. First, as shown in Section 3.4, high H_2:NO_x ratios favor the formation of NH_3 from the NO + H_2 reaction. Second, since the oxidation of NH_3 in the reaction front by adsorbed NO_x or O_2 proceeds in direct competition with the NO_x + H_2 and O_2 + H_2 reactions, increasing the H_2 concentration will favor the latter reactions, causing more NH_3 to break through the catalyst. Similar reasoning can be applied to the effect of the NO_x loading on NH_3 selectivity. The observation that NH_3 selectivity decreases with increasing NO_x loading suggests that the H_2:NO_x ratio in the reaction front exerts a major influence, i.e., as the NO_x concentration is increased, so the H_2:NO_x ratio decreases, favoring N_2 formation over NH_3. Furthermore, as the H_2:NO_x ratio decreases, relatively more NO_x should slip through the reaction front, and, after re-adsorption, be available for NH_3 consumption in the SCR reaction. Hence, NH_3 emissions should decrease.

The effect of space velocity on NH_3 selectivity must also be considered. One possible explanation for the observed increase in NH_3 selectivity with increasing GHSV involves the relative rates of the propagation of the reductant front through the catalyst and the rate of reverse spillover (transport of NO_x from the storage sites to the precious metal sites). At high space velocities the reductant front will propagate rapidly; therefore, by the time released NO_x reaches the precious metal sites, the front will have passed by and the NO_x will experience high local H_2 concentrations, favoring the formation of NH_3. Similar reasoning has been advanced by Harold and co-workers [48] to explain the increase in NH_3 selectivity observed with decreasing Pt dispersion in model LNT catalysts: decreased Pt-Ba contact at decreasing Pt dispersion results in slower kinetics of NO_x release and/or transport relative to the rate of propagation of the reductant front and hence higher local H_2:NO_x ratios. In the present work, it is also conceivable that the rates of the reactions of NH_3 with stored NO_x and O_2 could be kinetically limited at high space velocities; this would result in decreased consumption of NH_3 in the reductant front and hence higher NH_3 concentrations in the reactor effluent. Finally, it should be noted that at low space velocities the NSR zone will be concentrated in the front of the catalyst [32,33,46] (reflecting the fact that NO_x storage proceeds largely

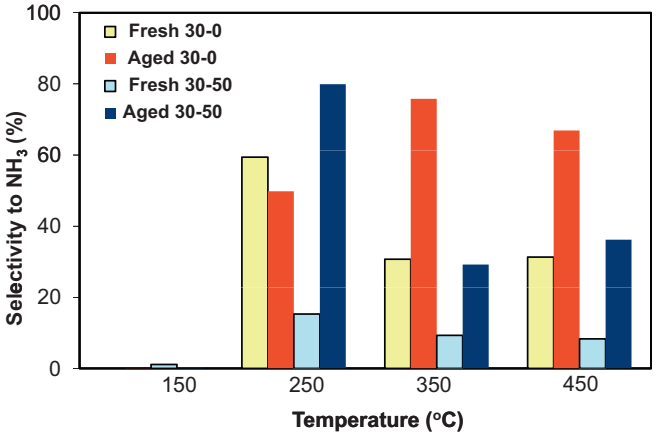

Fig. 9. Selectivity to NH_3 shown by fresh (de-greened) and aged catalysts 30-0 and 30-50 at different temperatures. Conditions as for Table 2; aging protocol as detailed in Section 2.2.

in a chromatographic-like fashion), whereas high space velocities can be expected to "stretch" the NSR zone along the length of the catalyst monolith. Consequently, increasing the GHSV will tend to move NH_3 formation deeper into the catalyst with the result that formed NH_3 will have less opportunity to react with NO_x or O_2 stored in the rear of the catalyst. This situation is somewhat analogous to that for aged catalysts, which is discussed in Section 3.8. Given the integral nature of catalyst monoliths, ascertaining the relative importance of these different effects is difficult based on reactor data alone; further clarification requires the use of techniques such as SpaciMS which can provide spatio and temporal resolution of the data.

Finally, an explanation must be sought for the strong temperature dependence of NO_x reduction. In this case, two factors appear to be of importance. First, it has been shown that H_2 is a better NO_x reductant than NH_3 at low temperatures [47]. Consequently, as the temperature is increased, the NO_x–NH_3 reaction becomes competitive with the NO_x–H_2 reaction, resulting in a relative increase in NH_3 consumption in the reductant front. Second, according to the results of a recent modeling study reported by Bhatia et al. [49], NH_3 generation is favored under conditions where diffusion of stored NO_x within the Ba phase to the Pt/Ba interface is the rate determining process (giving rise to fast reductant breakthrough and high H_2:NO_x concentrations at the Pt/Ba interface). Since NO_x diffusivity increases with increasing temperature [49], at higher temperatures the reductant feed rate, rather than the NO_x solid-phase diffusion rate, becomes limiting. Consequently, the reductant takes longer to break through, local H_2:NO_x concentrations are relatively lower, and the selectivity of NO_x reduction to N_2 is increased.

3.9. *Effect of catalyst aging—SpaciMS measurements*

As shown in Fig. 9, after aging selectivity to NH_3 is generally increased for 30-0 and 30-50, particularly at 350 and 450 °C. As we have noted previously [30,31], there are a number of possible factors which can account for this increase:

(i) Pt sintering (as shown in Table 3), which results in a decrease in the Pt–Ba interfacial perimeter, i.e., Pt–Ba phase segregation occurs upon aging. Hence, the rate of transport of stored NO_x to Pt sites during regeneration (reverse NO_x spillover) is decreased. If this rate is slower than the H_2 feed rate, then H_2 will break through with substantially more NO_x remaining on the catalyst after H_2 breakthrough. Consequently, the Pt surface will be predominantly covered by hydrogen, and as the stored NO_x transports to the Pt particles, NH_3 will be preferentially formed [48]. As mentioned above, recent modeling studies by Bhatia et al. [49] confirm this idea: NH_3 formation is favored when solid-phase diffusion of NO_x to the Pt/Ba interface is the rate determining process, which becomes increasingly likely as the Pt dispersion decreases.

(ii) The decreased OSC of the aged catalysts (see Table 3) should result in decreased reductant consumption by stored oxygen and hence higher effective H_2:NO_x ratios in the reductant front. Furthermore, there is less oxygen available downstream of the reductant front to react with formed NH_3.

(iii) After aging, the NO_x storage capacities of the catalysts are decreased (as reported previously [30,31]), i.e., there are fewer active sites available per unit of catalyst volume, which should result in higher effective H_2:NO_x ratios in the reductant front.

(iv) As the catalyst ages, the length of the NO_x storage-reduction zone increases due to the decrease in NO_x storage capacity. The longer the NSR zone, the shorter the downstream OSC-only zone (i.e., axial LNT portion free of stored NO_x) [32,33]. This leads to decreased oxidation of NH_3, slipping from the upstream NSR-zone, by oxygen stored in the OSC-only zone. Consequently, more NH_3 escapes from the LNT without being oxidized.

(v) A further possibility that must be considered pertains to the rates of the NO_x–NH_3 SCR and NH_3–O_2 reactions. If the rates are sufficiently decreased after aging, then NH_3 consumption via reaction with NO_x and O_2 stored downstream of the reaction front may be decreased, resulting in higher NH_3 emissions.

As noted above, the integral nature of monolith reactors greatly complicates the interpretation of reactor data. Therefore, in an effort to confirm the importance of the above factors, SpaciMS measurements [50,51] were performed on fresh and aged 30-0. It should be noted that the catalyst aging conditions employed for these measurements (see Section 2.6) were different to those used for the cycling experiments discussed above in Section 3.8, however, the maximum temperatures experienced during aging were similar (respectively, 800 °C under lean conditions and 770 °C under lean/rich conditions), and so the effects are expected to be qualitatively similar. Fig. 10 shows two-dimensional representations of NH_3 concentrations measured – as a function of time – at six different positions along the length of the catalyst monoliths during a single regeneration event. In both cases the regeneration event commenced at around 31.5 s and lasted 5 s. It should also be noted that the catalyst sample was 1″ (25.4 mm) in length; hence, the profile corresponding to 25.4 mm represents the NH_3 concentration measured at the outlet face of the monolith. For the fresh (de-greened) sample, the NO_x storage-reduction zone is largely confined to the front of the catalyst. This is evidenced by the corresponding NO_x release profiles, showing that the maximum gas phase NO_x concentration is attained near the front of the catalyst (data not shown). Consequently, the gas phase NH_3 concentration increases along the length of the NO_x storage-reduction zone peak, attaining its peak value towards the end of the zone (close to the middle of the catalyst in the axial direction). Subsequently, the NH_3 concentration diminishes due to its consumption by reaction with stored oxygen in the rear of the catalyst, as well as with any stored NO_x present and released NO_x that re-adsorbs on the catalyst downstream of the reductant front. It is also worth noting there that is a considerable delay in the evolution of NH_3 at the successive measurement points in the catalyst. This is indicative of a high level of H_2 and NH_3 consumption in the reductant front due to reaction with stored NO_x and O_2, meaning that the front propagates fairly slowly through the catalyst. This interpretation is consistent with SpaciMS data collected on a commercial LNT by Partridge and Choi [46], who similarly found that the NH_3 onset time systematically

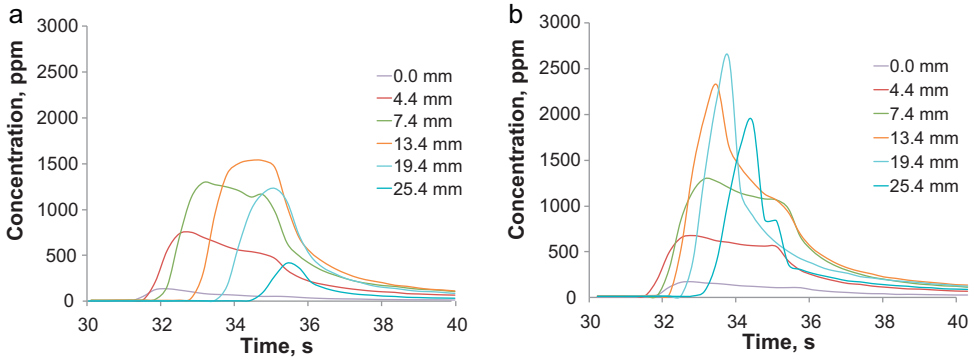

Fig. 10. Spatiotemporal NH_3 profiles for (a) de-greened and (b) aged catalyst 30-0, corresponding to a single 5 s regeneration event. 4.2% H_2 as reductant, 250 °C, other conditions as for Table 2.

shifts to later regeneration times with increasing distance into the catalyst, and that it tracks the shift in the H_2 onset time.

The above findings contrast with the situation for the aged catalyst. After aging, the time lag for the appearance of NH_3 is greatly decreased, indicating that the reductant front moves rapidly through the catalyst; this can be attributed to the lower amount of NO_x and O_2 stored in the front of the catalyst. Evidence that the NO_x storage-reduction zone is stretched along the length of the catalyst is also provided by the observation that the maximum NO_x gas phase concentration is attained near the center of the monolith (in the axial direction; data not shown) and that the maximum NH_3 concentration is attained approximately three-quarters of the way along the monolith (Fig. 10). In other words, the maxima for both NO_x and NH_3 release are moved towards the rear of the catalyst. As indicated above, this lengthening of the NO_x storage-reduction zone is a consequence of the fact that after aging there are fewer storage sites available per unit of catalyst volume. This, in turn, results in decreased oxidation of NH_3 by oxygen stored in the OSC-only zone, with the result that more NH_3 escapes from the LNT without being oxidized. Similar reasoning applies to the NH_3–NO_x reaction; since the concentration of gas phase NO_x peaks further along the catalyst, there are fewer storage sites downstream of the reductant front on which the NO_x can re-adsorb and subsequently undergo reaction with NH_3 present in the reductant front. Furthermore, it is also apparent that the peak NH_3 concentrations attained at the different measurement points in the catalyst are significantly higher after aging, consistent with a higher reductant:NO_x ratio (and hence higher selectivity of NO_x reduction to NH_3), and/or decreased rate of the NO_x–NH_3 reaction in the reaction front, resulting in less NH_3 consumption in the reaction front as it propagates along the monolith.

To summarize, these findings confirm that after aging the NSR zone is stretched along the catalyst, moving the peak NH_3 concentration further into the catalyst and providing less opportunity for NH_3 consumption by stored O_2 and NO_x downstream of the reductant front. Although the higher intracatalyst NH_3 concentrations measured after aging suggest that the intrinsic selectivity to NH_3 is increased as a consequence of the increased local H_2:NO_x ratio at the precious metal sites, higher NH_3 concentrations can also be explained by a decrease in the rate of the NO_x–NH_3 SCR reaction. Distinguishing between these possibilities will require quantitative analysis of the spatio-temporal data using appropriate models [52]. Such work is on-going in our laboratory.

4. Conclusions

In this study, the selectivity of NO_x reduction over fully formulated monolithic LNT catalysts was investigated as a function of the regeneration conditions. The following effects were identified:

- When using $CO + H_2$ as the reductant, selectivity to NH_3 (at a given temperature) increased with increasing regeneration time, reductant concentration and space velocity. The effect of these parameters on NH_3 selectivity can be interpreted largely in terms of the local H_2:NO_x ratio at the precious metal sites.
- Catalyst oxygen storage capacity was also found to be important in determining the selectivity of NO_x reduction to NH_3. This is attributed to two main effects: stored oxygen can consume part of the H_2 in the reductant front, thereby decreasing the effective H_2:NO_x ratio, and can also consume formed NH_3 via oxidation, giving N_2 as the main product.
- When using propene as the reductant, NH_3 selectivity was governed by the steam reforming activity of the LNT; hence, selectivity to NH_3 increased with increasing temperature and was slightly higher for the ceria-containing catalyst compared to its ceria-free analog.
- After aging, the catalysts displayed increased selectivity to NH_3; this is attributed in part to lengthening of the NO_x storage-reduction zone, resulting in decreased NH_3 consumption by NO_x and O_2 downstream of the reductant front. In addition, higher intracatalyst NH_3 concentrations measured after aging suggest that selectivity to NH_3 is increased as a consequence of the increased effective H_2:NO_x ratio at the precious metal sites. However, higher NH_3 concentrations can also be explained by a decrease in the rate of the NO_x–NH_3 SCR reaction.

Finally, it should be noted that in this work, excess H_2 was present during reduction of the stored NO_x. Under CO-rich, H_2-deficient conditions it can be anticipated that NH_3 formation will proceed to some degree via an isocyanate route [53], in which case the selectivity of NO_x reduction to NH_3 may follow somewhat different trends to those observed here.

Disclaimer

Acknowledgements

This project was funded by the U.S. Department of Energy (DOE) under award No. DE-EE0000205 and by Ford Motor Co. under the auspices of the Ford University Research Program.

References

[1] H. Hu, J. Reuter, J. Yan, J. McCarthy Jr., SAE Technical Paper 2006-01-3552 (2006).
[2] K.E. Bevan, W. Taylor III, SAE Technical Paper 2006-01-3551 (2006).
[3] R. Roecker, R. Zhan, R.H. Stanglmaier, SAE Technical Paper 2007-01-3983 (2007).
[4] R. Snow, G. Cavatatio, D. Dobson, C. Montreuil, R. Hammerle, SAE Technical Paper 2007-01-1244 (2007).
[5] R. Snow, D. Dobson, R. Hammerle, S. Katare, SAE Technical Paper 2007-01-0469 (2007).
[6] T. Nakatsuji, M. Matsubara, J. Rouistenmäki, N. Sato, H. Ohno, Appl. Catal. B 77 (2007) 190.
[7] H. Shinjoh, N. Takahashi, K. Yokota, Top. Catal. 42–43 (2007) 215.
[8] X. Chen, J. Schwank, Top. Catal. 46 (2007) 39.
[9] E.C. Dykes, SAE Technical Paper 2008-01-2642 (2008).
[10] E.C. Corbos, M. Haneda, X. Courtois, P. Marecot, D. Duprez, H. Hamada, Catal. Commun. 10 (2008) 137–141.
[11] E.C. Corbos, M. Haneda, X. Courtois, P. Marecot, D. Duprez, H. Hamada, Appl. Catal. A 365 (2009) 187.
[12] L. Xu, R. McCabe, W. Ruona, G. Cavataio, SAE Technical Paper 2009-01-0285 (2009).
[13] M. Weibel, N. Waldbüsser, R. Wunsch, D. Chatterjee, B. Bandl-Konrad, B. Krutzsch, Top. Catal. 52 (2009) 1702.
[14] R. Zukerman, L. Vradman, M. Herskowitz, E. Liverts, M. Liverts, A. Massner, M. Weibel, J.F. Brilhac, P.G. Blakeman, L.J. Peace, Chem. Eng. J. 155 (2009) 419.
[15] D. Chatterjee, P. Koči, V. Schmeisser, M. Marek, M. Weibel, B. Krutzsch, Catal. Today 151 (2010) 395.
[16] R. Bonzi, L. Lietti, L. Castoldi, P. Forzatti, Catal. Today 151 (2010) 376.
[17] P. Forzatti, L. Lietti, Catal. Today 155 (2010) 131.
[18] A. Lindholm, H. Sjövall, L. Olsson, Appl. Catal. B 98 (2010) 112.
[19] J.A. Pihl, J.E. Parks II, C.S. Daw, T.W. Root, SAE Technical Paper 2006-01-3441 (2006).
[20] J. Xu, R.D. Clayton, V. Balakotaiah, M.P. Harold, Appl. Catal. B 77 (2008) 395.
[21] R.D. Clayton, M.P. Harold, V. Balakotaiah, Appl. Catal. B 81 (2008) 161.
[22] J. Siera, B.E. Nieuwenhuys, H. Hirano, T. Yamada, K.I. Tanaka, Catal. Lett. 3 (1989) 179.
[23] S. Hackenberg, M. Ranalli, SAE Paper 2007-01-1239 (2007).
[24] I. Nova, L. Castoldi, L. Lietti, E. Tronconi, P. Forzatti, Top. Catal. 42–43 (2007) 21.
[25] M. Abdul-Milh, H. Westberg, Top. Catal. 42–43 (2007) 209.
[26] M. AL-Harbi, W.S. Epling, Appl. Catal. B 89 (2009) 315.
[27] A. Kouakou, F. Dhainaut, P. Granger, F. Fresnet, I. Louis-Rose, Top. Catal. 52 (2009) 1734.
[28] Y. Ji, T.J. Toops, M. Crocker, Catal. Lett. 119 (2007) 257.
[29] Y. Ji, J. Choi, T.J. Toops, M. Crocker, M. Naseri, Catal. Today 136 (2008) 146.
[30] Y. Ji, C. Fisk, V. Easterling, U. Graham, A. Poole, M. Crocker, J.-S. Choi, W.P. Partridge, K. Wilson, Catal. Today 151 (2010) 362.
[31] Y. Ji, V. Easterling, U. Graham, C. Fisk, M. Crocker, J.-S. Choi, Appl. Catal. B 103 (2011) 413.
[32] J.-S. Choi, W.P. Partridge, C.S. Daw, Appl. Catal. B 77 (2007) 145.
[33] J.-S. Choi, W.P. Partridge, J.A. Pihl, C.S. Daw, Catal. Today 136 (2008) 173.
[34] J. Sjoblom, K. Papadakis, D. Creaser, C.U.I. Odenbrand, Catal. Today 100 (2005) 243.
[35] P. Jozsa, E. Jobson, M. Larsson, Top. Catal. 30–31 (2004) 177.
[36] D. James, E. Fourre, M. Ishii, M. Bowker, Appl. Catal. B 45 (2003) 147.
[37] S. Poulston, R.R. Rajaram, Catal. Today 81 (2003) 603.
[38] T. Lesage, C. Verrier, P. Bazin, J. Saussey, M. Daturi, Phys. Chem. Chem. Phys. 5 (2003) 4435.
[39] Z. Liu, J.A. Anderson, J. Catal. 224 (2004) 18.
[40] M. AL-Harbi, D. Radtke, W.S. Epling, Appl. Catal. B 96 (2010) 524.
[41] R. Burch, J. Breen, F. Meunier, Appl. Catal. B 39 (2002) 283.
[42] E. Joubert, X. Courtois, P. Marecot, C. Canaff, D. Duprez, J. Catal. 243 (2006) 252.
[43] S.S. Mulla, S.S. Chaugule, A. Yezerets, N.W. Currier, W.N. Delgass, F.H. Ribeiro, Catal. Today 136 (2008) 136.
[44] L. Cumaranatunge, S.S. Mulla, A. Yezerets, N.W. Currier, W.N. Delgass, F.H. Ribeiro, J. Catal. 246 (2007) 29.
[45] L. Lietti, I. Nova, P. Forzatti, J. Catal. 257 (2008) 270.
[46] W.P. Partridge, J.-S. Choi, Appl. Catal. B 91 (2009) 144.
[47] R.D. Clayton, M.P. Harold, V. Balakotaiah, Appl. Catal. B 84 (2008) 616.
[48] R.D. Clayton, M.P. Harold, V. Balakotaiah, C.Z. Wan, Appl. Catal. B 90 (2009) 662.
[49] D. Bhatia, M.P. Harold, V. Balakotaiah, Catal. Today 151 (2010) 314.
[50] J.-S. Choi, W.P. Partridge, C.S. Daw, Appl. Catal. A 293 (2005) 24.
[51] J.-S. Choi, W.P. Partridge, W.S. Epling, N.W. Currier, T.M. Yonushonis, Catal. Today 114 (2006) 102.
[52] D. Bhatia, R.D. Clayton, M.P. Harold, V. Balakotaiah, Catal. Today 147 (2009) 250.
[53] T. Szailer, J.H. Kwak, D.H. Kim, J.C. Hanson, C.H.F. Peden, J. Szanyi, J. Catal. 239 (2006) 51.